On the Effect of Antenna Calibration Errors on Geodetic Estimates

Investigation on Zero and Double Difference Approaches

Tobias Kersten, Grzegorz Krzan, Karol Dawidowicz, and Steffen Schön

Abstract

This paper addresses an approach to assess the impact of phase centre correction errors of selected receiving antennas in the Polish ASG-Eupos network using GNSS processing strategies such as zero differencing and double differencing. The objective is to characterise the nature of the error patterns of GNSS receiver antennas and to understand their impact on GNSS derived integrated water vapour and geodetic estimates. A semi-analytical approach for characterising variants of error patterns is applied. Differences of up to +12 mm between type-mean and individual receiver antenna calibrations of current antenna models on the ionosphere-free linear combination are identified for repeatable pattern deformations. The analyses show that repeatable effects on tropospheric estimates of up to 8 mm – which corresponds to approx. 1.2 kg/m^2 – occur even though only 5 mm variations were applied to the pattern. The results of our analysis show a strong correlation with the type of error patterns that affect the estimates differently. Due to the complex relationship between datum settings, processing strategy, baseline orientation and satellite sky distribution, artefacts in GNSS processing models and their effects must to be modelled in order to achieve a better understanding in the context of GNSS networks and GNSS meteorology.

Keywords

Coordinates · Double difference (DD) · Generic patterns · Phase centre corrections (PCC) · Zenith tropospheric delays (ZTD) · Zero difference (ZD)

1 Introduction

Meteorology and climate monitoring are crucial to both tracking and monitoring extreme weather phenomena and understanding of climate change and its impact. The Global Navigation Satellite System (GNSS) – starting with GPS (Tralli et al. 1992) – serves since the early 1990s as one of several observation techniques to derive a vertical profile of water vapour content and its composition in the lower atmosphere (troposphere). This provides important information about the structure of the monitoring of our most important greenhouse gas.

Several GNSS networks provide atmospheric products for global weather forecasting or monitoring of humidity in the lower atmosphere as an absolute measure, e.g. the International GNSS Service (IGS), the European Permanent Network (EPN) or the Global Climate upper air reference network (GRUAN, Vaquero-Martinez et al. 2019).

Bock and Parracho (2019) found biases in the time series of integrated water vapor (IWV) between 1–4 kg/m^2 with a standard deviation of below 2 kg/m^2 and also showed a strong relation between geographical, topographical and climatic features and demonstrated persistence of small-scale variability despite a reanalysis.

T. Kersten (✉) · S. Schön
Leibniz University Hannover, Institut für Erdmessung (IfE), Hannover, Germany

G. Krzan · K. Dawidowicz
University of Warmia and Mazury (UWM), Olsztyn, Poland

J. T. Freymueller, L. Sánchez (eds.), *Geodesy for a Sustainable Earth*,
International Association of Geodesy Symposia 154, https://doi.org/10.1007/1345_2022_153

Ning et al. (2016) pointed out the challenge of deriving GNSS troposphere estimates that satisfy the demands of climate research. It is worth noting that data processing artefacts and imperfect models are easily introduced into the tropospheric estimates leading, e.g. to artificial trends of up to 0.15 kg/(m^2 year). Nguyen et al. (2021) show the effect of different *a priori* models for the hydrostatic zenith delay that are as critical as the quality of the antenna/radome calibrations and applied mapping functions.

There are two techniques to achieve receiver antenna corrections. The first is a calibration in an anechoic chamber (Zeimetz and Kuhlmann 2008) using synthetic signals and the second is a robot arm that uses in-situ available GNSS radio signals (Menge et al. 1998). In general, good comparability below 1–2 mm phase differences was found between both techniques and selected antennas. But also higher differences of 4–6 mm are reported among the methods (Krzan et al. 2020). This magnitude occur also between type mean and individual calibrations. Systematic deviations that occur significantly reduce the achievable quality as a result of the very complex interactions of GNSS antennas with their entire environment and location. The impact of PCCs inaccuracies on geodetic and meteorological estimates strongly relies on: (1) the concept and philosophy of implemented processing approach, (2) the types of applied observations or linear combinations used, (3) the number and type of parameters estimated, (4) the mapping function chosen, and (5) the local satellite coverage, i.e the geographic location. Santerre et al. (2017) emphasised the impact of the local sky distribution. Douša et al. (2016) stressed the need of consistent and accurate GNSS carrier phase centre corrections (PCCs) for satellite and receiver antennas to monitor severe weather events and climate. Vey et al. (2009) reported magnitudes of up to ± 1 kg/m^2 due to antenna and radome changes in GPS IWV time series, which is related to approx. ± 7 mm variation in the zenith total delay (ZTD).

The complex interaction of PCCs and the troposphere underlines the need to assess the quality and reliability of PCC sets for receiving antennas on both frequently used GNSS processing strategies, the zero difference (ZD, Zumberge et al. 1997) approach and the double difference (DD, Odijk and Wanninger 2017) approach.

Since neither the cause of the error effect of the receiver patterns nor their influence on the estimates are sufficiently well known, this paper sheds light on the complex interaction with tropospheric parameters in order to better answer the important question of the required accuracy and the impact of the receiver antennas on the absolute GNSS IWV estimates.

2 Troposphere and Antenna Phase Centre Calibrations

2.1 Troposphere Estimates

GNSS radio signal refraction in the troposphere is frequency independent and subsequently has to be modelled and estimated in terms of signal delay. According to Davis et al. (1985), two parts are combined to the ZTD, the hydrostatic delay (ZTD_h) and the moisture (wet) delay (ZTD_w) such as

$$ZTD = ZTD_h \cdot f_h(e) + ZTD_w \cdot f_w(e) \tag{1}$$

where ZTD_h is the *a priori* model for hydrostatic part, $f_h(e)$ and $f_w(e)$ reflect the mapping function for the dry and wet part, respectively, and e denotes the elevation angle. The ZTDs are linked to the Integrated Water Vapour (IWV, in kg/m^2) or the Predictable Water Vapour (PWV, in mm) by transformation with additional measures, i.e. temperature and atmospheric pressure, taking into account uncertainty measures (Bevis et al. 1992). In addition, Beutler et al. (1988) explored how ZTDs correlate with station height by a factor of 1:−3, meaning that 1 mm error in the troposphere modelling results in a −3 mm offset in station height. These relations negatively affect the accuracy, precision, and homogeneity of GNSS ZTD and PWV/IWV time series.

.

2.2 Antenna Phase Centre Calibrations

The antenna PCCs are essential for high accuracy processing since the calibration values define the location of the GNSS antenna phase centre. This is not a common fixed location but rather a surface that varies with the properties of the antenna, the entire surrounding. The PCCs are defined as a function of local azimuth ϕ and elevation θ angle, frequency f, GNSS system s. They are separated into a mean phase centre offset (PCO) and phase centre variations (PCVs)

$$PCC_{s,f}(\phi,\theta) = -\mathbf{e}^T \mathbf{PCO}_{s,f} + PCV_{s,f}(\phi,\theta) + r_{s,f} \tag{2}$$

with the unit line-of-sight vector $\mathbf{e}$ to the satellite and $r_{s,f}$ expressing the one degree of freedom (Rothacher et al. 1995).

The results of calibration methods – whether in anechoic chambers or on robotic arms – are sets of gridded correction values presented in ANTEX format (Rothacher and Schmid 2010). While the effect of type mean or individual calibration on station coordinates is discussed on global and regional scales (Araszkiewicz and Völksen 2016; Villiger et al. 2020; Krzan et al. 2020), there is a need to assess the impact of

the accuracy of PCC patterns on meteorological parameters in order to provide uncertainty bounds for e.g. ZTDs and understand sources of bias in IWV time series.

2.3 Issues of Receiver Antenna Patterns

To illustrate the current challenges, our study analysis a set of representative receiving antennas from a regional network (Polish ASG-EUPOS), which are summarised in Table 1 and depicted in Fig. 1. The individual PCCs are retrieved from the network operator's website (ASG EUPOS 2021), while the corresponding type means origin from IGS (IGS CB 2021)

Differences of type means and individual antenna calibrations can easily reach levels of more than ±1 mm on each frequency, which is an international accepted consensus (so called *rule-of-thumb*). By applying the ionosphere-free (L0) linear combination as needed for regional and global GNSS processing, these differences increase rapidly.

The analysis of elevation-only dependent ΔPCCs can mislead the comparison as examples in Fig. 2 indicate. There, different pattern structures are identified with systematic repetitions. Figure 2a shows deviations below 4 mm except a wobble at 135° azimuth. The ΔPCC pattern also shows a repeated ring structure with magnitudes of +3 mm. Regard-

Table 1 Stations of AGS-EUPOS network and related receive antenna equipment used in this setup

Station	Antenna	Dome	Serial No.	Cal.-Date
BYDG	TRM59900.00	SCIS	5347361485	2014-06-12
CHHN	TRM55971.00	TZGD	36334	2007-10-31
DAZI	TRM59900.00	SCIS	5317361068	2014-09-23
GNIE	LEIAR20	LEIM	17098001	2015-09-30
GRUD	TRM55971.00	TZGD	77056	2007-11-13
ILAW	TRM55971.00	TZGD	36524	2007-10-26
KONI	LEIAR20	LEIM	18208017	2015-10-02
KUTN	TRM59900.00	SCIS	5316361054	2014-09-19
SOCH	TRM55971.00	TZGD	36130	2010-02-18
WLOC	TRM55971.00	TZGD	1440929151	2010-02-17

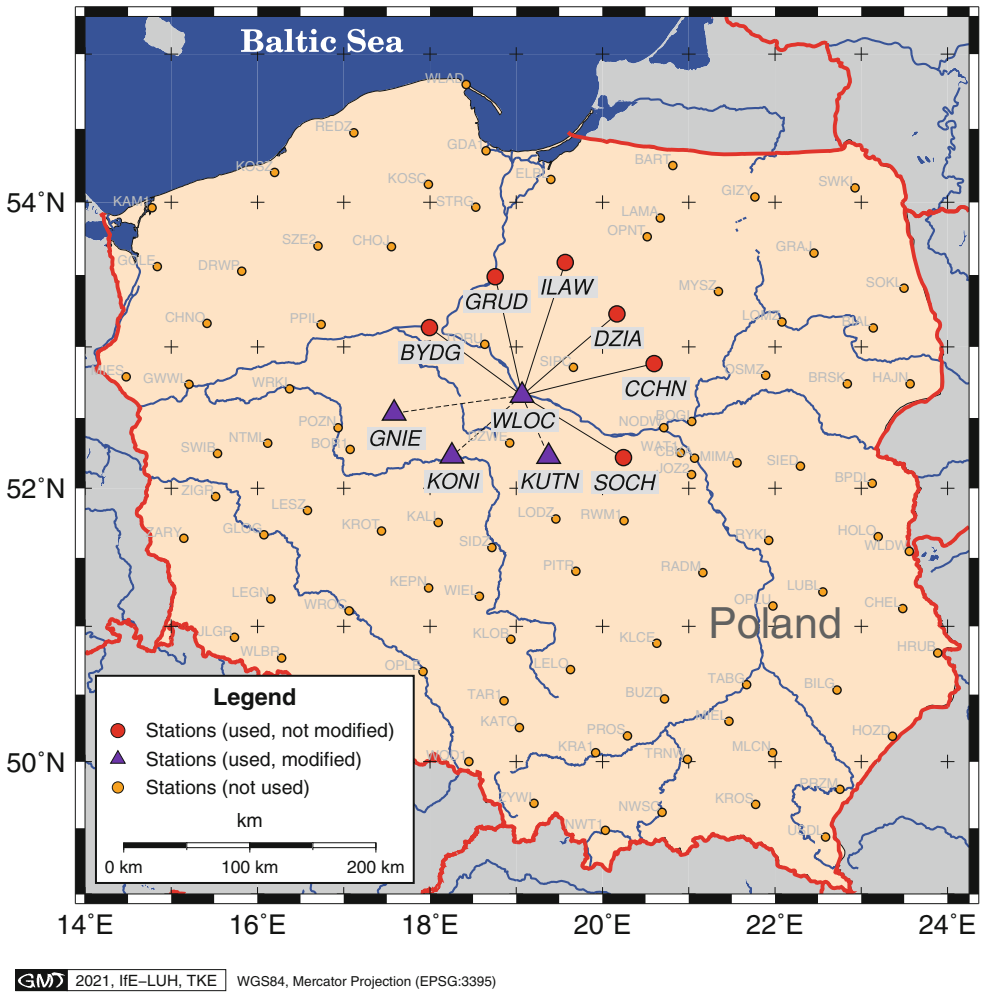

Fig. 1 Network to assess deviations between PCC models on a minimum constraint network

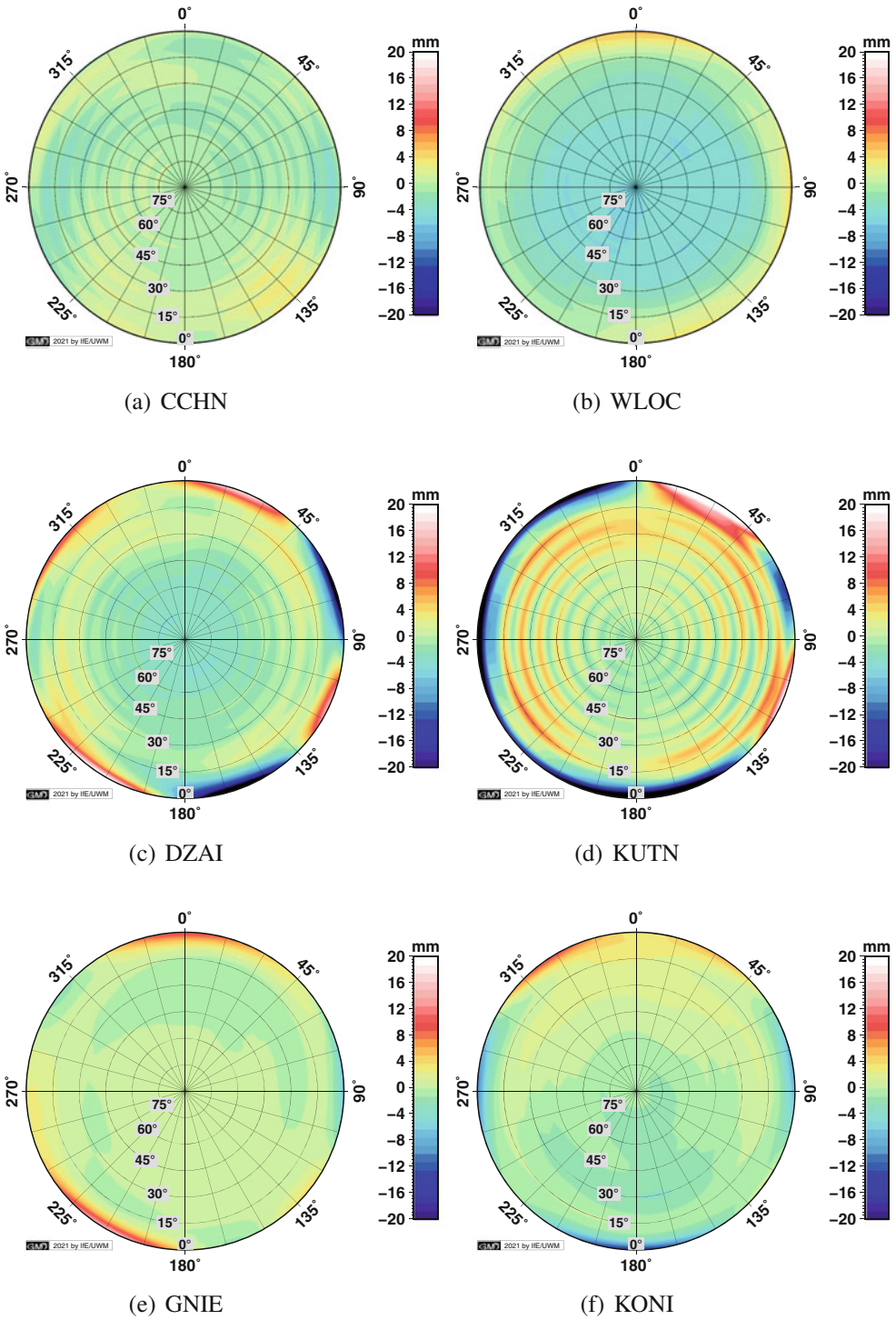

(a) CCHN (b) WLOC

(c) DZAI (d) KUTN

(e) GNIE (f) KONI

Fig. 2 Differential PCC (ΔPCC) pattern for ionosphere-free linear-combination between type-mean and individual calibrations for different receiver antennas, (**a**,**b**) TRM55971.00 TZGD, (**c**,**d**) TRM59900.00 SCIS and (**e**,**f**) LEIAR20 LEIM

ing Fig. 2d, such structure appears again for approx. every 15° elevation angle with magnitudes of +8 mm that occur – despite higher deviations below 5° elevation – also at mid-elevation.

Smaller but systematic deviations between 4–6 mm are detected for the other groups of GNSS antennas with not symmetrically distributed deviations. This indicates that for different geographic locations those pattern topologies (cf. Fig. 2) will have non-negligible effect above 5° elevation angle.

Mean L0 biases for ΔPCC (type mean vs. individual calibrations) vary in our study per group (i.e. antenna model) and overall between −3.6 mm and +2.0 mm for individual antennas (cf. Table 2).

An alternative metric for the comparison of two patterns is the range $\Delta_{min}^{max}\{PCC\}$ of the differences that considers the

variation with the azimuth and elevation angle (cf. Table 2). In the case of individual ΔPCCs, ranges at L0 with magnitudes of 8 mm up to 22.5 mm are detected.

Those variations are projected through zero difference (ZD) processing, e.g. in Precise Point Positioning (PPP, Zumberge et al. 1997), onto the estimated parameters.

In the case of differential GNSS data processing, such as double difference (DD), a different scenario results, as ΔPCCs from two independent antennas i and j are now combined to form a new set, such as

$$\delta\Delta PCC = \Delta PCC_i - \Delta PCC_j, \tag{3}$$

Table 2 Summary of mean L0 ΔPCC pattern for both individual antenna patterns and difference patterns on selected baselines w.r.t WLOC

	Mean L0 bias		L0 Range	
Station	ΔPCC [mm]	$\delta\Delta PCC^{i}_{WLOC}$ [mm]	ΔPCC [mm]	$\delta\Delta PCC^{i}_{WLOC}$ [mm]
BYDG	−2.4	−3.9	8.5	10.5
CHHN	1.1	−0.4	8.0	8.8
DAZI	−1.8	−3.1	13.3	15.9
GNIE	0.2	−1.5	5.4	12.3
GRUD	0.6	−0.8	9.9	9.9
ILAW	1.1	−0.4	10.5	9.2
KONI	−1.2	−2.8	11.8	16.9
KUTN	−3.6	−5.0	22.5	21.5
SOCH	2.0	0.5	10.4	8.9
WLOC	1.4	–	7.9	–

where the resulting effect can be understood as a baseline-specific antenna. Figure 3 shows this relation for the case of pure elevation dependent differences $\delta\Delta$PCCs for several baselines with respect to station WLOC (cf. Fig. 1 and Table 1). For some baselines, the $\delta\Delta$PCCs do not exceed three millimetres. However, at elevation angles of 15° significant deviations of up to −10 mm occur if only the elevation dependent $\delta\Delta$PCC are considered, or up to −12 mm if the ranges of azimuthal deviations are also considered. By correlating the mean number of available observations with the distribution of realistic satellite constellation for mid latitude located ground stations (cf. Fig. 3), the largest deviation of the $\delta\Delta$PCC pattern on L0 occurs at elevation angles with the highest number of expected observations (5500–4000 at 15–30° elevation range), considering an elevation dependent weighting. Menge et al. (1998) describe the effect of an erroneous pattern in terms of geographical location and baseline length.

It is worth noting that the analysis of elevation dependent PCCs can lead to significant misinterpretations of the pattern deviations. Hence, they only can serve as an initial indicator (cf. Table 2). They do not provide reliable benchmarks for comprehensive quality assessment.

Examining the range metric for L0 in Table 2, the smallest deviations result from the fact that the same antenna type (TRM55971.00 TZGD) is combined when forming the baseline (mean L0 bias of −0.8 mm to +0.5 mm with a corresponding range of 9–10 mm). Larger

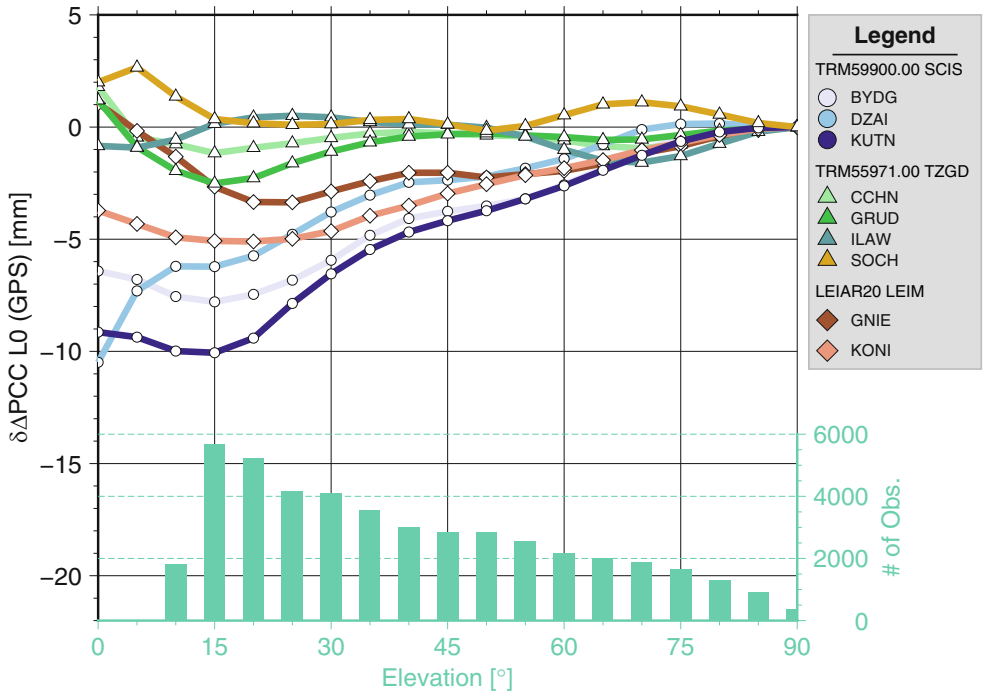

Fig. 3 Individual derivations of elevation dependent ΔPCCs for analysed baselines and their mean distribution of maximal number of observations per elevation bin

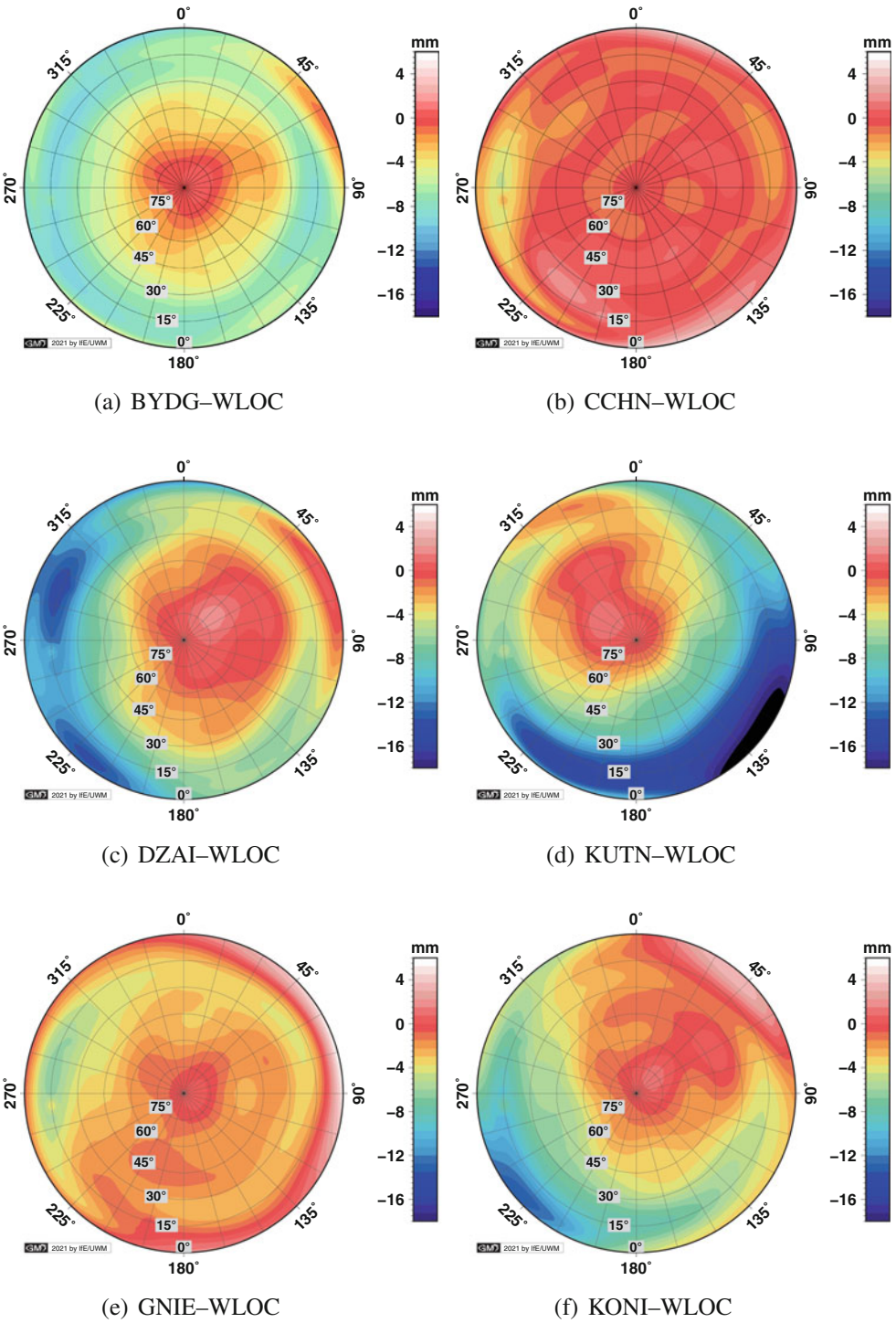

(a) BYDG–WLOC (b) CCHN–WLOC

(c) DZAI–WLOC (d) KUTN–WLOC

(e) GNIE–WLOC (f) KONI–WLOC

Fig. 4 Different receiver antennas baseline specific $\delta\Delta$PCC for ionosphere-free (L0) linear combination for type mean and individual calibrations with respect to WLOC, (**a**,**b**) TRM55971.00 TZGD, (**c**,**d**) TRM59900.00 SCIS and (**e**,**f**) LEIAR20 LEIM

deviations are caused by different antenna models (cf. Table 2).

Azimuth and elevation angle dependent $\delta\Delta$PCCs are provided in Fig. 4, highlighting that deviations for CCHN can vary from −4 mm to +4 mm in the best case. Larger deviations are also reported, which results in systematic effects. This is shown, for example, in a $\Delta h \sin\theta$ effect, with $\Delta h = -8$ mm at the station BYDG. For the stations DZAI, KUTN and KONI a shift of the pattern from 0 mm to −12 mm is found as well. On the contrary, a twist is present at GNIE (cf. Fig. 4). These features occur regularly, suggesting that modelling of these components by measures of the generic pattern (Geiger 1988; Kersten and Schön 2016) is beneficial to assess the appropriate type and characteristics of the resulting impact.

3 Modelling and Assessing GNSS Antenna Variability

3.1 Generic Patterns

Two approaches are possible to assess the effect of different PCC patterns: (1) applying the two patterns (individual and type mean PCCs) in the processing and analysing the effect on the parameters, or (2) modelling the ΔPCC and $\delta\Delta$PCC for the corresponding processing strategy, such as ZD and DD, and achieve a numerical model for typical characteristics. In this paper, we apply the second approach for a case study – following a semi-analytical approach.

Analytical formulations of generic patterns are introduced by Geiger (1988). They are parameterised by continuous integral functions with parameters for the local azimuth λ and elevation angle θ that results in a range error $\delta\delta r(\lambda, \theta)$. Considering the findings from Sect. 2.3, we validate selected generic patterns (cf. Table 3). Characteristics and magnitudes of pattern variability are resulting from previous section (cf. Table 2).

One and four-wire model applies to study asymmetrical structures as

$$\begin{aligned}\delta\delta r(\theta,\lambda) =& A\sin\theta \\ &+ D\cdot\sin\theta\cos\left(N\lambda + (p4W\theta - Na_0)\right)\end{aligned} \tag{4}$$

with amplitudes A and D, the number of wires N, the polarisation p of the antenna (corresponding to $p = -1$ for right hand circular polarised) and the number of wingdings $W \equiv 1$, and the initial azimuth $a_0 = 0$. The parameter N applies for the one/four-wire model ($N = 1/4$).

Chess board is a regular pattern in λ with factors for cosine and sine functions cl, sl and in θ with factors ct, st that are applied in

$$\delta\delta r(\theta,\lambda) = A\left(\cos ct\theta\right)\sin\left(st\theta\right)\cos(cl\lambda)\cos\left(sl\lambda\right)) \tag{5}$$

to interpret and model the variability of PCC patterns.

3.2 Methodology and Evaluation

The original PCC patterns are applied as regular using the ANTEX format. The modified patterns PCC* are applied by considering the range errors $\delta\delta r(\theta, \lambda)$ on the individual patterns using Eq. (2) for selected station i like

$$\{PCC^*_{s,f}\}_i = \{PCC_{s,f}\}_i + \delta\delta r, \tag{6}$$

which are shown in Fig. 1. These $\{PCC^*_{s,f}\}_i$ are also formulated in ANTEX format and are applied accordingly in the GNSS processing. As a result, this study seeks to answer the question of whether the semi-analytical method provides enough information to analyse the effects of the antennas with sufficient accuracy to justify continuing towards a purely analytical approach in future.

Following the requirements of a realistic scenario, selected sites (approx. 35%) in a network of at least ten GNSS stations (cf. Fig. 1) are modified. The stations are selected to be at similar altitude, circularly distributed, and having similar baseline lengthsrelative to the centre station Włocławec (WLOC). The network is adjusted using minimum constraint datum.

The GNSS data processing for ten consecutive days applies for both, ZD (estimation strategy) using the NAPEOS GNSS Software (Springer and Dow 2009), and DD (elimination strategy) using Bernese GNSS Software (Dach et al. 2015). Close similar configurations are used in the processing of the data in a normal equation batch strategy. In NAPEOS, the ZTDs are modelled with Saastamoinen (Saastamoinen 1972) and Global Pressure and Temperature (GPT) model and as mapping function the corresponding global mapping function (GMF). In Bernese, we apply the dry Vienna Mapping Function (VMF, Boehm et al. 2006) as the ZTD model and for the wet part the corresponding VMF wet mapping function. In both cases the resolution of the ZTDs is one hour with loose absolute and relative constraints. The impact of antenna variability was analysed by comparing the modified network solution against a reference solution, derived by applying individual PCC corrections for all ten days.

Table 3 Model parameters for generic patterns in the analysis study

No	Model	A [mm]	N []	D [mm]	Chess board ct []	cl []	st = sl []
1	One-wire helix	5	1	5	–	–	–
2	Four-wire helix	5	1	5	–	–	–
3	Four-wire helix	20	1	5	–	–	–
4	Chess board	5	–	–	7	3	1

4 Results

4.1 Position Domain

The variability of the receiver antenna PCCs are analysed for both ZD and DD processing approach and result in similar solutions. The applied error pattern introduce affine distortions to the processed network for all studied cases through the chosen datum setting (minimum constraint). This is illustrated in Fig. 5 by the combined ten days solution on the coordinate domain. While the asymmetrical case of one-wire helix (model 1, cf. Fig. 5a) leads to deviation in the topocentric North, East and Up component, this is not the case for the symmetrical patterns (cf. Fig. 5c) as the

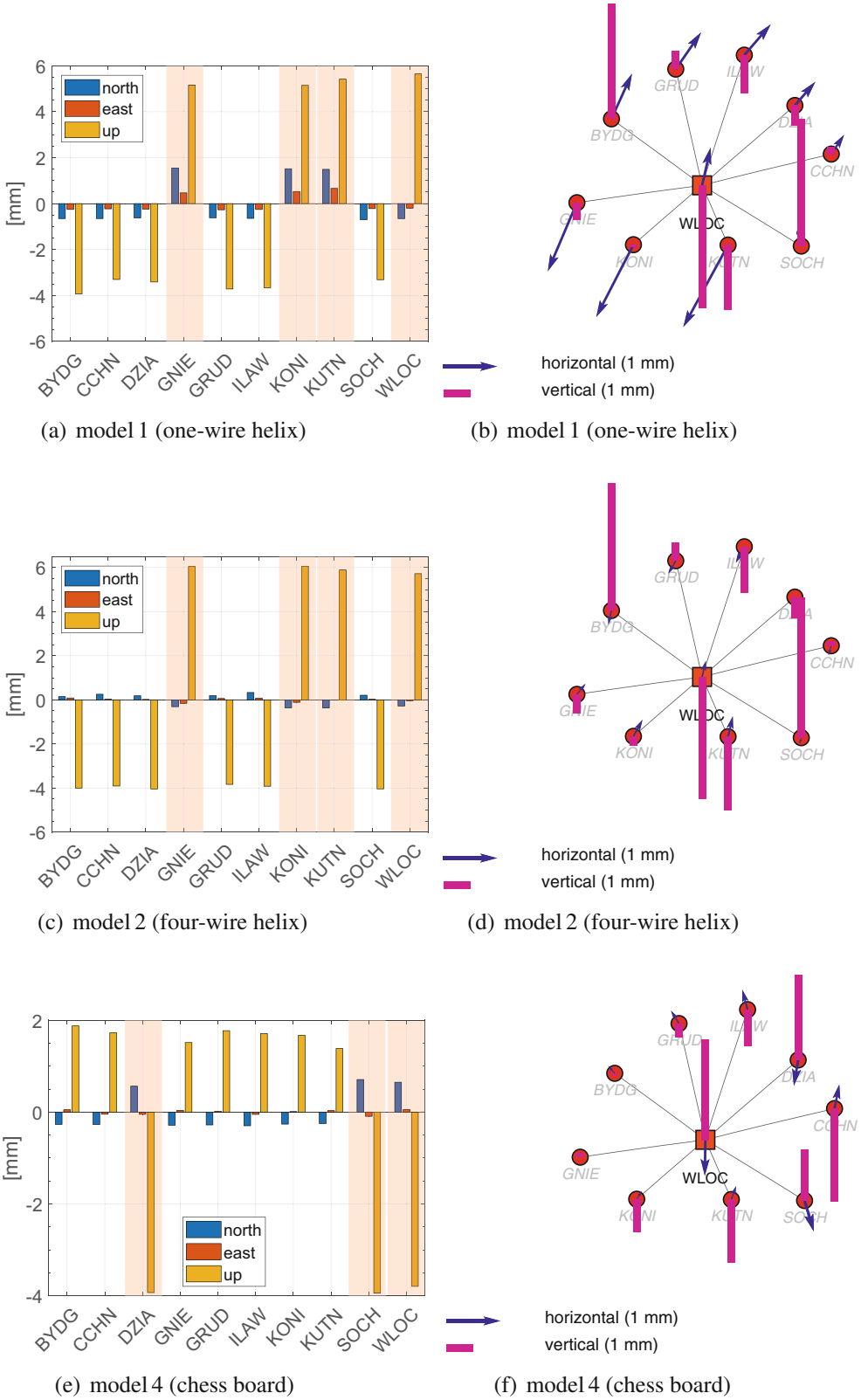

(a) model 1 (one-wire helix) (b) model 1 (one-wire helix)

(c) model 2 (four-wire helix) (d) model 2 (four-wire helix)

(e) model 4 (chess board) (f) model 4 (chess board)

Fig. 5 Results of combined network solution for individual models and modified PCCs for positions (**a**, **c**, **e**) and network distortion as residuals after a 3d Helmert transformation (**b**, **d**, **f**). Shaded backgrounds in (**a**, **c**, **e**) indicate the stations that were modified with pre-defined generic patterns

effect is projected in majority to the Up component. This relationship became apparent through the effects on the overall geometry of the network, as shown in Figs. 5b, d and f for the residuals of a 3d Helmert transformation with respect to the reference solution. Because of the minimum constraint datum, the effects of the modified stations in the

network will be absorbed by all the non-modified stations. This leads to the effect that all unmodified stations will show a negative offset that is the result of the sum of all effected stations divided by the number of all unaffected stations. Example: in Fig. 5c an impact on the Up component of +6 mm is introduced, leading to a magnitude of 24 mm which is distributed by all 6 unmodified stations that result to an offset of −4 mm in the Up component. Those findings are close similar to achieve for the other studied models, but the effect in the Up component varies slightly due to additional effects on the horizontal components.

The characteristic of the deformed pattern also leads to a deformation of the overall network geometry, as shown in Fig. 5b. There, the network enlarges towards the northeast and southwest, resulting in a scaling effect that has its origin in the centre of the network. However, the scaling has more effect on the position estimates and less on the ZTDs, as the impact on the Up component is different. Nevertheless, the spatial distribution of the effects in the Up component of the network is important to know, as it will affect the spatial distribution of the ZTDs and thus the PWV/IWV derivatives.

Table 4 Summary of results for the ZTD time series estimates versus the reference solution for the models 1–3; the asterisk mark correspond to those stations where modified PCC patterns were applied

	Model 1		Model 2		Model 3	
	Bias [mm]	RMS [mm]	Bias [mm]	RMS [mm]	Bias [mm]	RMS [mm]
BYDG	0.2	2.2	−0.4	3.7	−2.0	3.2
CCHN	0.4	2.2	−0.5	3.7	−1.8	3.2
DZAI	0.3	2.1	−0.5	3.7	−2.0	3.3
GNIE*	1.1	2.6	0.9	3.7	2.2	3.9
GRUD	0.3	2.1	−0.4	3.7	−2.0	3.2
ILAW	0.2	2.1	−0.4	3.7	−1.9	3.2
KONI*	1.2	2.5	0.8	3.7	2.0	3.5
KUTN*	1.2	2.5	0.9	3.7	2.2	3.7
SOCH	0.4	2.1	−0.5	3.7	−1.9	3.2
WLOC*	1.5	2.5	0.8	3.7	1.7	3.5

4.2 Troposphere Parameters

The effects on the tropospheric parameters are in close relation to the network geometry and thus the effects of the Up component. An explanation gives Fig. 6 for statistical metrics, such as cumulative histogram and quantile graphs. The asymmetrical case of one-wire helix (model 1) affects all position components (height and horizontal), leading into variations below 4 mm for approx. 95% of ZTDs (cf. Fig. 6a). Assuming a symmetrical pattern with exactly the same magnitude of distortion leads to higher deviations, so that only 80% of all ZTDs of less than 4 mm are affected, but higher values of up to 8 mm definitely appear (cf. Fig. 6b). Assuming a gross error in the patterns (amplitude of 20 mm, model 3) results again to the fact that 95% of ZTD biases are below 4 mm for the non-affected stations (cf. Fig. 6c), but now the impact of affected antennas on the network is separated. The smallest impact is detected for model 4 – a asymmetrical variation with regular variations along azimuth and elevation angles – that results to variation of ZTDs of below 3 mm in 95% of all ZTDs.

The effect that is introduced by modified PCCs seems to be normal distributed in a first approximation at least between ±1.5 mm (cf. Figs. 6e–h). However, in the case of model 2 (cf. Fig. 6f) and model 4 (cf. Fig. 6h) not only an offset was detected but also a systematic variation. The offsets found in the quantile graphs are in correspondence to the magnitudes listed in Table 4. The RMS values of model 1 are quite small with 2.2 mm and show only marginal differences for the affected stations (cf. Table 4). It is worth noting that the noise of the ZTDs gets also affected by the kind of applied generic pattern, which indicates a close relation between the characteristic of error contribution on the pattern and effect on the estimated ZTDs.

5 Conclusions

In this contribution, we have shown that deviations and defects in the PCC patterns are likely to have significant effects on the position level and on estimated ZTDs. With this study, there is a contribution to trace the error on the pattern and assign the impact in order to gain more understanding on the current shortcomings of GNSS water vapour time series – i.e. to gather information on the cause and effect. Currently, such variations are found, for example, between type mean and individual calibrations, which have different magnitudes and pattern characteristics. For instance, we have shown that frequency dependent deviations are significantly amplified with the L0 linear combination, so that the effects on the PCC patterns easily reach up to 12 mm. Likewise, we have been able to assign repeatable pattern variations. Our work has also shown that a pure elevation dependent representation is neither adequate nor beneficial to qualitatively describe the variability of the variations.

The structure of PCC patterns are the key to applying analytical functions for describing these variations. To learn how each PCC topology behaves in GNSS data processing – taking into account the satellite geometry – we processed the patterns in ZD and DD and compared the results with respect to the ZTDs.

Because of high correlation of the Up component and ZTDs, similarities are found. Depending on the patterns, non-normally distributed deviations have been identified on the ZTDs, which are related to the type of introduced distortion and show deviations of up to 8 mm. The effect on the

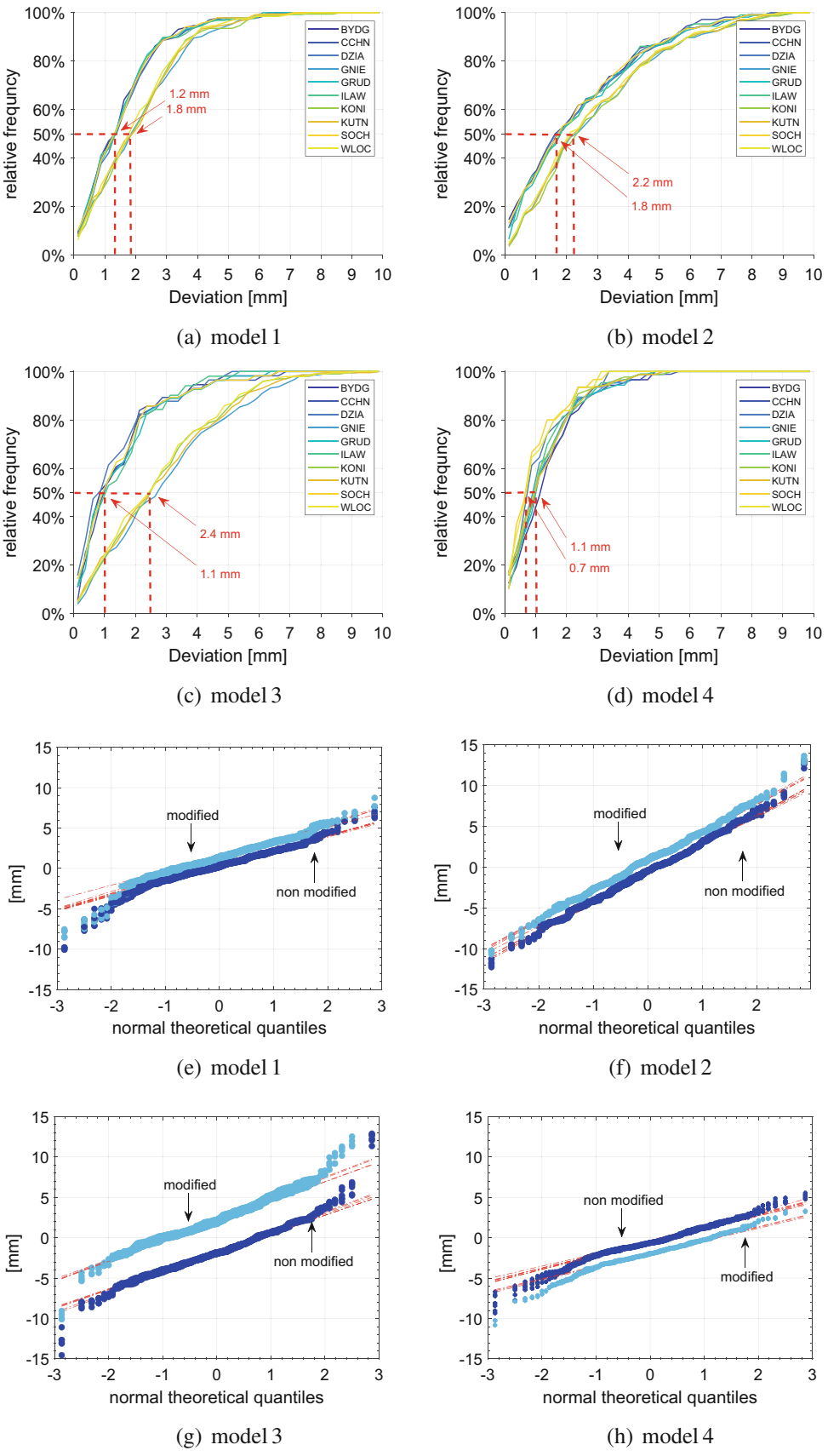

(a) model 1 (b) model 2

(c) model 3 (d) model 4

(e) model 1 (f) model 2

(g) model 3 (h) model 4

Fig. 6 Variations of ZTDs by cumulative histograms (**a**–**d**) and quantile representation (**e**–**h**) considering a minimum constraint datum

ZTDs is also strongly depending on the selected datum and varies accordingly.

Consequently, future models need to take into account the datum setting in addition to the analytical description of the antenna deviation and the underlying satellite geometry.

Acknowledgements The authors grateful acknowledge the Polish ASG-EUPOS network providers for the ANTEX antenna and RINEX observation files from their network. We also thank the Centre of Orbit Determination in Europe (CODE) and the European Space Operations Centre (ESOC) at ESA, which provide high accurate GNSS products.

References

Araszkiewicz A, Völksen C (2016) The impact of the antenna phase center models on the coordinates in the EUREF permanent network. GPS Solut 21(2):747–757. https://doi.org/10.1007/s10291-016-0564-7

ASG EUPOS (2021) https://www.asgeupos.pl

Beutler G, Bauersima I, Gurtner W, Rothacher M, Schildknecht T, Geiger A (1988) Atmospheric effects on geodetic space measurements, chap Atmospheric refraction and other important biases in GPS carrier phase observations, pp 15–43

Bevis M, Businger S, Herring T, Rocken C, Anthes R, Ware R (1992) GPS meteorology: Remote sensing of atmospheric water vapor using the Global Positioning System. J Geophys Res 97:15787–15801

Bock O, Parracho AC (2019) Consistency and representativeness of integrated water vapour from ground-based GPS observations and ERA-interim reanalysis. ACP 19(14):9453–9468. https://doi.org/10.5194/acp-19-9453-2019

Boehm J, Werl B, Schuh H (2006) Troposphere mapping functions for GPS and very long baseline interferometry from European Centre for Medium-Range Weather Forecasts Operational Analysis Data. J Geophys Res 111(B2):B02406. https://doi.org/10.1029/2005JB003629

Dach R, Lutz S, Walser P, Fridez P (eds) (2015) Bernese GNSS software version 5.2. University of Bern, Bern Open Publishing. https://doi.org/10.7892/boris.72297

Davis JL, Herring TA, Shapiro II, Rogers AEE, Elgered G (1985) Geodesy by radio interferometry: Effects of atmospheric modeling errors on estimates of baseline length. Radio Sci 20(6):1593–1607. https://doi.org/10.1029/rs020i006p01593

Douša J, Dick G, Kačmařík M, Brožková R, Zus F, Brenot H, Stoycheva A, Möller G, Kaplon J (2016) Benchmark campaign and case study episode in central Europe for development and assessment of advanced GNSS tropospheric models and products. Atmos Meas Tech 9(7):2989–3008. https://doi.org/10.5194/amt-9-2989-2016

Geiger A (1988) Modeling of phase centre variation and its influence on GPS-positioning. In: GPS-techniques applied to geodesy and surveying. Lecture Notes in Earth Sciences, vol 19. Springer, pp 210–222. https://doi.org/10.1007/BFb0011339

IGS CB (2021) https://igs.org/

Kersten T, Schön S (2016) Receiver antenna phase center models and their impact on geodetic parameters. In: IAG Symposia, vol 147. Springer, Cham, pp 253–259. https://doi.org/10.1007/1345_2016_233

Krzan G, Dawidowicz K, Wielgosz P (2020) Antenna phase center correction differences from robot and chamber calibrations: The case study LEIAR25. GPS Solutions 24(2). https://doi.org/10.1007/s10291-020-0957-5

Menge F, Seeber G, Völksen C, Wübbena G, Schmitz M (1998) Results of the absolute field calibration of GPS antenna PCV. In: ION GPS 1998, Sept. 15–18, Nashville, TN, USA, pp 31–38

Nguyen KN, Quarello A, Bock O, Lebarbier E (2021) Sensitivity of change-point detection and trend estimates to GNSS IWV time series properties. Atm 12(9):1102. https://doi.org/10.3390/atmos12091102

Ning T, Wickert J, Deng Z, Heise S, Dick G, Vey S, Schöne T (2016) Homogenized time series of the atmospheric water vapor content obtained from the GNSS reprocessed data. J Clim 29(7):2443–2456. https://doi.org/10.1175/JCLI-D-15-0158.1

Odijk D, Wanninger L (2017) Differential positioning. In: Springer Handbook of global navigation satellite systems. Springer, pp 753–780. https://doi.org/10.1007/978-3-319-42928-1_26

Rothacher M, Schmid R (2010) ANTEX: The antenna exchange format, Version 1.4. https://files.igs.org/pub/data/format/antex14.txt

Rothacher M, Schaer S, Mervat L, Beutler G (1995) Determination of antenna phase center variations using GPS data. In: IGS workshop, 15–18 May, Potsdam, Germany

Saastamoinen J (1972) Contributions to the theory of atmospheric refraction. Bull géodésique 105(1):279–298. https://doi.org/10.1007/BF02521844

Santerre R, Geiger A, Banville S (2017) Geometry of GPS dilution of precision: revisited. GPS Solut 21(4):1747–1763. https://doi.org/10.1007/s10291-017-0649-y

Springer T, Dow JM (2009) NAPEOS–mathematical models and algorithms. Tech. rep., European Space Agency (ESA/ESOC, Darmstadt)

Tralli DM, Lichten SM, Herring TA (1992) Comparison of Kalman filter estimates of zenith atmospheric path delays using the Global Positioning System and very long baseline interferometry. Radio Sci 27(6):999–1007. https://doi.org/10.1029/92rs01779

Vaquero-Martinez J, Antón M, de Galisteo JPO, Román R, Cachorro VE, Mateos D (2019) Comparison of integrated water vapor from GNSS and radiosounding at four GRUAN stations. Sci Total Environ 648:1639–1648. https://doi.org/10.1016/j.scitotenv.2018.08.192

Vey S, Dietrich R, Fritsche M, Rülke A, Steigenberger P, Rothacher M (2009) On the homogeneity and interpretation of precipitable water time series derived from global GPS observations. J Geophys Res 114(D10). https://doi.org/10.1029/2008JD010415

Villiger A, Dach R, Schaer S, Prange L, Zimmermann F, Kuhlmann H, Wübbena G, Schmitz M, Beutler G, Jäggi A (2020) GNSS scale determination using calibrated receiver and Galileo satellite antenna patterns. J Geod 94(9). https://doi.org/10.1007/s00190-020-01417-0

Zeimetz P, Kuhlmann H (2008) On the accuracy of absolute GNSS antenna calibration and the conception of a New Anechoic chamber. In: FIG working week 2008 - Integrating generations, June 14–19, Stockholm, Sweden, p 16

Zumberge JF, Heflin MB, Jefferson DC, Watkins MM, Webb FH (1997) Precise point positioning for the efficient and robust analysis of GPS data from large networks. J Geophys Res 102(B3):5005–5017. https://doi.org/10.1029/96JB03860